Cell-Specific Regulation of Intestinal Immunity in *Drosophila*.

Minjeong Shin, Lena Ocampo Jones, Kristina Petkau, Andrew Panteluk, Edan Foley[1].

Department of Medical Microbiology and Immunology, Faculty of Medicine and Dentistry, University of Alberta, Edmonton, AB T6G 2S2, Canada.

1: Corresponding author.

Edan Foley: efoley@ualberta.ca

ABSTRACT

The intestinal epithelium contains secretory and absorptive cell lineages that are derived from undifferentiated progenitor cells. Despite the collective importance of these cells to host responses against microbial invaders, little is about the contributions of immune responses in individual cell types to the maintenance of intestinal homeostasis. In this study, we asked how inhibition of immune pathway activity exclusively in progenitor cells, or in differentiated enterocytes, affects midgut homeostasis in adult *Drosophila*. We found that blocking immune activity in enterocytes rendered flies more tolerant of *Vibrio cholerae* infection, had negligible effects on the gut bacterial microbiome, and significantly affected metabolism. In contrast, inhibition of immune activity in progenitors rendered flies less tolerant of *Vibrio* infections, modified host association with *Lactobacillus* symbionts, and blocked growth and renewal in the midgut epithelium. Together, these data uncover substantial cell type-specific contributions of epithelial immunity to the maintenance of adult intestinal homeostasis.

INTRODUCTION

The intestine processes a mixture of ingested materials that contain essential nutrients, but may also be tainted with harmful toxins or microbes. To extract nutrient and limit tissue damage, intestinal homeostasis requires the coordinated actions of immune and metabolic responses within the epithelium. The epithelium is maintained by progenitor cells that divide and differentiate to generate secretory, or absorptive cells that act in regionally specialized manners. For example, the anterior intestinal epithelium contains defined regions of low pH, and areas characterized by the expression of digestive enzymes that degrade complex, bulky material. In contrast, posterior epithelial cells are typically responsible for the uptake of small molecules, such as water and electrolytes.

In addition to digestion, the epithelium is also critical for the neutralization of threats posed by resident, or transitory microbes (1). Antimicrobial defenses include physical barriers constructed from polymeric materials, such as mucins or the chitinous peritrophic matrix, as well as tight cell-cell contacts that prevent paracellular leakage of potentially harmful molecules. In addition to barrier defenses, host-derived reactive oxygen species eliminate invasive microbes in a rather indiscriminate manner that can also lead to collateral damage of host tissue. Finally, immune systems rely on intra- and extracellular receptors that survey the intestinal environment for molecular patterns of the gut microbial content (2). Detection of microbial signatures activates defenses tailored to prevent microbial invasion of the host interior.

Although we understand many host signaling pathways that respond to intestinal microbes, we have less information about how the engagement of immune pathways in specific cell types contribute to the immune response. *Drosophila melanogaster* is a valuable system to address this question. The fly posterior midgut shares numerous similarities with the vertebrate small intestine, and is highly amenable to the modification of gene expression in defined intestinal cells (3). Similar to vertebrates, the fly midgut is maintained by a basal population of progenitor cells composed of intestinal stem cells that typically divide asymmetrically to generate a new stem cell and a transient cell type – the enteroblast (4, 5). Enteroblasts frequently respond to signals from the Notch pathway to generate absorptive enterocytes (6, 7), a differentiated cell type that undergoes several rounds of

endoreplication to produce large cells that occupy the majority of the midgut cellular volume. Less frequently, stem cells generate secretory enteroendocrine cells, either indirectly via enteroblasts that do not receive Notch signals, or more directly via an enteroendocrine intermediary (8–10). As with vertebrates, stem cell division is regulated by mitogenic cues from pathways that include EGF, Wnt, and JAK-STAT, and the rate of ISC division is tuned to the rate of epithelial damage (11, 12). In the absence of an extrinsic stressor, stem cells divide approximately once every two weeks in adult females (4, 13). However, damage to the midgut activates repair pathways that shift ISC proliferation rates. In this case, molecular cues from damaged cells accelerate ISC division. This burst of progenitor growth generates a pool of cells that replenishes damaged structures and maintains the epithelial barrier.

In contrast to the advances made in understanding the contribution of individual cell types to epithelial renewal, we know less about cell-specific regulation of intestinal immunity. The Immune Deficiency (IMD) pathway, a germline-encoded antibacterial defense with numerous similarities to the mammalian TNF pathway (14), is activated by detection of bacterial DAP-type peptidoglycan (PGN) (15, 16). IMD regulates approximately 50% of the intestinal transcriptional response to the microbiota (17), and alterations in immune activity are associated with effects on the composition and load of the gut microbiota (16–20). Similar to digestive processes, the IMD pathway displays hallmarks of cellular, and regional specialization (21–23). In the anterior of the intestine, IMD activation requires the extracellular receptor, PGRP-LC, that detects polymeric PGN, and antibacterial defenses appear to be predominantly activated in large, differentiated cells (24). In the posterior midgut, IMD activation requires PGRP-LE (24, 25), an intracellular sensor that detects monomeric PGN (26), and IMD pathway components are expressed and activated in undifferentiated progenitor cells (27–29), as well as terminally differentiated enterocytes.

Despite these regional and cellular distinctions in IMD activation, we do not know how IMD acts in individual cell types to regulate intestinal homeostasis. To address this question, we generated a *Drosophila* line that allows cell-specific inhibition of IMD. With this line, we determined the physiological consequences of IMD inactivation exclusively in progenitors or in enterocytes. Our results revealed significant differences between the contributions

of enterocyte IMD and progenitor IMD to intestinal homeostasis. Inhibition of IMD in enterocytes extended the lifespan of adults challenged with pathogenic *Vibrio cholerae*, did not affect composition of the intestinal microbiome, but had significant effects on host metabolism. In contrast, inhibition of IMD in progenitors shortened the lifespan of flies challenged with *Vibrio cholerae*, impacted the representation of *Lactobacillus* symbionts within the microbiota, and significantly impaired the growth of intestinal stem cells. Combined these data uncover fundamental differences between the impacts of immune activity in progenitor cells, and their differentiated progeny.

RESULTS

Cell-specific effects of IMD on host responses to bacterial infection

To determine cell-specific contributions of IMD to intestinal homeostasis, we developed a transgenic fly line that allows inducible inhibition of IMD in defined cell types. In *Drosophila*, IMD activation requires proteolytic removal of the N-terminal thirty amino acids from the Imd protein by the caspase Dredd, and expression a non-cleavable Imd (ImdD30A) prevents signal transduction through the IMD pathway (30). Consistent with these data, we found that expression of ImdD30A in the adult fat body completely blocked the infection-dependent expression of the IMD-responsive antimicrobial peptide, *diptericin* (Fig. 1A). We used this transgenic fly line to ask how cell-sepcific inactivation of IMD impacts host survival after with oral infection with *V.cholerae*, a pathogenic bacteria that kills adult flies in a manner that includes contributions from the IMD pathway (31, 32). To answer this question, we used the TARGET gene expression system (33) to express ImdD30A exclusively in intestinal progenitors (*esg^{ts}/D30A*), or in differentiated enterocytes (*Myo1A^{ts}/D30A*). When we blocked IMD exclusively in progenitor cells, we found that flies infected with *V. cholerae* died significantly faster than control *esg^{ts}/+* flies (Fig. 1B). Conversely, enterocyte-specific suppression of IMD extended the survival of infected flies relative to control *Myo1A^{ts}/+* flies (Fig. 1C). As *esg^{ts}/D30A* flies and *Myo1A^{ts}/D30A* flies respond differently to infection with *V. cholerae*, we asked if inhibition of IMD in progenitors or enterocytes had differential effects on host colonization by *V. cholerae*. Initially, we looked at the impacts of *esg^{ts}/D30A* and *Myo1A^{ts}/D30A* on feeding rates, a possible modifier of host colonization by *V. cholerae*. In Capillary Feeding (CAFE) assays, we found that *esg^{ts}/D30A* flies and *Myo1A^{ts}/D30A* flies consumed equal amounts of liquid food as their respective controls (Fig. 1 D and E). Furthermore, we found that expression of ImdD30A in enterocytes or in progenitors did not impact the consumption of solid food, as determined by a FlyPad assay (Supplementary Fig. 1). Finally, we detected equal loads of *V. cholerae* in *esg^{ts}/D30A* flies and *Myo1A^{ts}/D30A* flies relative to their respective controls (Fig. 1 F and G). In sum, our data suggests that IMD has cell-specific impacts on host tolerance of an enteric pathogen.

Effects of cell-specific IMD inactivation on the intestinal microbiome

The data above uncover cell-specific contributions of IMD to survival of infection with a pathogenic bacteria. This led us to ask if IMD acts in cell-specific manners to regulate interactions between the host and symbiotic bacteria. To answer this question, we first generated axenic populations of *esg^{ts}/+*, *esg^{ts}/D30A*, *Myo1A^{ts}/+* and *Myo1A^{ts}/D30A* embryos (Fig. 2A). Next, we raised axenic embryos at 21°C in sterile environment until adulthood to prevent unwanted expression of *imdD30A* during development. We fed axenic adults a homogenate prepared from our lab wild-type flies to ensure that all genotypes had a similar intestinal microbiome. We transferred flies from each group to 29°C for ten days to drive ImdD30A expression in progenitors (*esg^{ts}/D30A*) or enterocytes (*Myo1A^{ts}/D30A*). Finally, we performed triplicate 16S deep-sequencing analyses of the intestinal microbiome in each genotype at days five and twenty-nine after association with a conventional microbiome. Of the 24 samples, 22 had sufficient read depth to allow us determine the overall composition of the gut bacterial microbiome. Principle component analysis (Fig. 2B), phylogenetic diversity metrics (Fig. 2C), and operational taxonomic unit analysis (Fig. 2D) all suggest that inactivation of IMD in differentiated enterocytes had minimal impact on the composition of the intestinal microbiome at both time points. In each case, we did not observe significant differences between bacterial populations in *Myo1A^{ts}/ImdD30A* flies, and their *Myo1A^{ts}/+* controls at either day 5 or day 29. In contrast, inactivation of IMD in progenitors appears to affect both the diversity (Fig. 2 B andC) and composition of the intestinal microbiome (Figure 2D), particularly at early stages. Here, we noted a relative increase in the amounts of *Lactobacillales* in five day-old *esg^{ts}/D30A* intestines relative to age-matched *esg^{ts}/+* controls. In older intestines, we observed a reverse effect (Fig. 2D). In this case, the relative abundance of *Lactobacillales* was lower in *esg^{ts}>D30A* populations (mean abundance: 8.1%), than in all other genotypes (mean abundance: 15.2%). We then generated balance trees to determine if cell-restricted inactivation of IMD affects the abundance of bacterial subcommunities within the intestinal microbiome. These studies identified a dominant balance that distinguished five day-old *esg^{ts}/D30A* intestines from all other genotypes (Fig. 2 E andF). Further examination of this group revealed a dominance of *Lactobacillales* and *Psudomonadales* within that balance. Combined, these data suggest cell-dependent contributions of IMD to host associations with *Lactobacillus* species:

inhibition of IMD in progenitor cells has an impact on the growth of *Lactobacillus* symbionts, while inhibition of IMD in enterocytes appears to have negligible effects.

Loss of IMD in progenitors affects association with symbiotic *Lactobacillus* species

Our 16S deep-sequencing data suggested differential effects of cell-restricted IMD inactivation on the relative proportions of intestinal symbionts in the fly (Fig. 2). To determine if IMD affects the total amounts of intestinal bacteria, we measured bacterial loads in flies with either progenitor or enterocyte-specific inactivation of IMD. For this experiment, we first standardized the bacterial composition associated with each fly lines. Specifically, we generated axenic embryos of all genotypes (*esg^{ts}/+*, *esg^{ts}/D30A*, *Myo1A^{ts}/+*, and *Myo1A^{ts}/D30A*) to eliminate the endogenous microbiome, and poly-associated the axenic adult flies with a 1:1:1 mix of three common fly symbionts – *Acetobacter pasteurianus* (*Ap*), *Lactobacillus brevis* (*Lb*), and *Lactobacillus plantarum* (*Lp*). We measured bacterial loads by serial dilution and counting of colony-forming units in adult flies that we raised at 29°C for 1, 10, 20, or 30 days. This approach allowed us to trace age-dependent changes in the microbiota of flies with compromised intestinal immune defenses. Consistent with our deep-sequencing data, enterocyte-specific suppression of IMD did not affect the load of any of the tested bacterial species at any of the tested time points, suggesting that loss of IMD in enterocytes alone does not have a detectable effect on either the load or relative proportions of common fly intestinal symbionts (Fig. 3A). Similarly, we did not observe measurable effects of IMD inhibition in progenitors on *Ap* loads at all times tested. In control *esg^{ts}/+* flies, the load of *Ap* gradually increased as flies aged to 20 days and dropped slightly in 30-day old flies (Fig. 3B). This pattern was also observed in flies with progenitor-specific suppression of IMD (*esg^{ts}/D30A*), and there were no significant differences in intestinal *Ap* numbers between the two genotypes at any of the times measured. In contrast, we detected age-dependent effects of IMD inhibition in progenitors on intestinal *Lactobacillus* numbers. For example, *Lb* load remained approximately the same up to 10 days in *esg^{ts}/+* and *esg^{ts}/D30A* flies and increased up to 1 X 10^6 CFU/fly in 30-day-old control flies (*esg^{ts}/+*). However, in *esg^{ts}/D30A* flies there was a significant decrease in the colony-forming units per fly of *Lb* at 30 days compared to *esg^{ts}/+* control flies of the same age (Fig. 3B). We noted similar effects

of IMD inhibition in progenitors on *Lp* numbers. Here, there was a significant drop in *Lp* loads at 30 days in *esg^{ts}/D30A* flies relative to their *esg^{ts}/+* controls (Fig. 3B). Combined with the data presented in Figure 2, our results suggest that IMD activity in progenitor cells contributes to the maintenance of intestinal *Lactobacillus* symbiont numbers as the fly ages.

Enterocyte IMD regulates metabolism and adult viability

Given the cell-specific impacts of IMD inactivation on host survival, microbiome composition, and symbiont load, we hypothesized that the IMD pathway exerts cell-specific controls on transcriptional events in the midgut. To test this hypothesis, we performed side by side RNA-sequencing of the transcriptome of guts with IMD specifically inactivated in enterocytes or intestinal progenitors. To understand how enterocyte IMD modifies intestinal function, we compared the transcriptomes of purified midguts from *Myo1A^{ts}/D30A* and control *Myo1A^{ts}/+* flies that we raised at 29°C for ten days (Fig. 4A). We found that inhibition of IMD in enterocytes had substantial effects on intestinal transcriptional activity (Fig. 4B, C), leading to modified expression of genes involved in a range of cellular processes (Fig. 4D). Unsurprisingly, the cohort of IMD-responsive genes includes immune effectors and modulators (Supplementary Fig. 2). However, we also found that inhibition of IMD in enterocytes had significant effects on processes as diverse as the control of cell shape, transport of metabolites, and metabolism of amino acids (Fig. 4D). These wide-ranging impacts prompted us to ask if inhibition of IMD in enterocytes affects metabolism in the fly. To answer this question, we examined glucose, trehalose and lipid levels in the intestines and carcasses of *Myo1A^{ts}/D30A* and *Myo1A^{ts}/+* flies that we incubated at 29°C for ten days. Inhibition of enterocyte IMD did not affect glucose levels in the whole fly, or in the intestine (Fig. 4 E and F). Likewise, inhibition of IMD in enterocytes did not affect trehalose, the main circulating disaccharide in the fly (Fig. 4G). In contrast, inhibition of IMD in enterocytes resulted in significant increases of total (Figure 4H), and intestinal triglyceride levels (Fig. 4I), as well as an increase in adult weight (Fig. 4J). These observations implicate enterocyte IMD in the control of triglyceride storage in the adult. Interestingly, a loss of function mutation in *imd* leads to decreased triglyceride levels (Supplementary Fig. 3), indicating enterocyte-specific roles for IMD in triglyceride

storage. As enterocyte IMD modifies several key processes such as metabolism in the intestine, we reasoned that inactivation of IMD will have consequences for intestinal physiology and animal viability. Consistent with this prediction, we found that blocking IMD in enterocytes impaired intestinal stem cell proliferation (Fig. 4J), and shortened adult lifespan (Fig. 4K). Combined, these results show that enterocyte IMD activity contributes to the regulation of adult viability and metabolism.

Progenitor-specific roles for IMD

In parallel to a transcriptional characterization of *Myo1A^{ts}/D30A* midguts, we determined the transcriptomes of purified midguts from *esg^{ts}/D30A* and *esg^{ts}/+* flies that we raised at 29°C for ten days. Again, we noticed significant impacts of IMD inhibition on the transcriptional activity of the midgut (Fig. 5 A and B), with consequences for a range of GO terms (Fig. 5C). Examination of GO terms affected by inhibition of IMD in progenitors revealed a partial overlap with GO terms affected by inhibition of IMD in enterocytes. For example, both manipulations had similar effects on the expression of genes linked to metabolism of amino acids or glutathione. However, IMD inhibition in progenitor cells had unique characteristics that were absent from the transcriptome of flies with inhibition of enterocyte IMD. For example inhibition of IMD in progenitors alone increased expression of genes involved in lipid catabolism and diminished expression of genes involved in RNA interference (Fig. 5C). In fact, greater than 30% of all genes impacted by IMD inhibition in progenitors were not affected by the inhibition of IMD in enterocytes (Fig. 5 D and E), suggesting unique roles for progenitor cell IMD activity in the gut. A close examination of genes differentially affected by inhibition of IMD in progenitor cells revealed the expected effects on immune response genes (Fig. 5F). We also noticed particularly striking impacts on the expression of genes required for cholesterol absorption and signaling; piRNA biogenesis; components of Notch, Wnt and JAK/STAT pathways; modifiers of proteostasis; and regulators of adult lifespan (Fig. 5F). We consider these alterations to gene expression particularly interesting, as many of the pathways are involved in progenitor cell homeostasis and aging (34–36). In combination, our transcriptional studies reveal large differences

between the contributions of enterocyte, or progenitor cell, IMD to intestinal homeostasis, and raise the possibility that progenitor cell IMD has roles in the growth and viability of intestinal stem cells.

IMD activity in progenitors promotes stem cell proliferation and *Drosophila* viability

Based on the effects of progenitor-specific suppression of IMD on pathways with roles in intestinal homeostasis and aging (Figure 5F), we hypothesized that progenitor-specific inhibition of IMD will affect the proliferation of intestinal stem cells and adult *Drosophila* lifespan. To directly quantify the effects of ImdD30A on intestinal stem cell populations, we first determined the proportion of stem cells in young and aged flies using Delta as a stem cell marker. We did not observe differences in the number of ISCs between 5-day-old *esg^{ts}/D30A* and control *esg^{ts}/+* flies (Fig. 6A). However, there was a significant decrease in the percent of Delta-positive cells in *esg^{ts}/D30A* flies compared to *esg^{ts}/+* control flies when flies were aged for 30 days (Fig. 6A). These results suggest that IMD activity promotes ISC proliferation in adult flies. In agreement with this hypothesis, we detected a significant decrease in proliferating cells in *esg^{ts}/D30A* flies when compared to *esg^{ts}/+* control flies (Fig. 6B). Together, our data suggest that IMD in progenitors is essential for the maintenance and growth of ISCs.

Given the impacts of IMD inhibition on progenitor renewal, we next tested the effect of progenitor-specific IMD suppression on longevity. For this experiment, we used the RU486-inducible GeneSwitch GAL4 system (33) to block IMD in progenitors. Using two independent *UASimdD30A* lines, we monitored and compared the lifespans of control flies to flies with progenitor-specific suppression of IMD. In both cases, we found that flies died significantly faster when IMD was blocked in progenitors in comparison to control flies (Fig. 6 C and D). Taken together, our data indicate that IMD activity in the progenitor compartment protects the fly from pathogenic *Vibrio cholerae*, supports the growth of symbiotic *Lactobacillus* species, and contributes to epithelial growth and adult longevity.

DISCUSSION

The intestine contains functionally distinct secretory and absorptive cell lineages that are replenished from a population of basal progenitor cells. These cells coordinate nutrient acquisition with immune defenses to support animal growth and survival. Disruptions to gut immunity permit the invasion of interstitial tissues by commensal microbes, leading to the onset of severe illnesses in the host (37). To fully understand how immune defenses restrict commensal microbes to the intestinal lumen, it is essential that we understand how individual cell types contribute to tissue-wide antibacterial defenses. We used *Drosophila melanogaster* to characterize the contributions of immune signaling in intestinal progenitors, or enterocytes, to intestinal homeostasis. Our study uncovered cell-specific contributions of IMD to host metabolism, intestinal growth, and the survival of enteric infection.

In *Drosophila*, DAP-type peptidoglycan activates the IMD response, a signal transduction pathway that displays hallmarks of regional specialization in the intestine (21–23). IMD has complex roles in the regulation of intestinal anti-bacterial responses (38). In the anterior, IMD activation occurs in differentiated epithelial cells upon detection of cell-extrinsic, polymeric peptidoglycan by PGRP-LC (24), leading to expression of antimicrobial peptides, presumably limiting the dissemination of ingested bacteria. In the posterior midgut, transcriptional and functional studies showed that IMD components are expressed and active in enterocytes and in progenitor cells (27–29), where IMD activation occurs upon detection of cytosolic, monomeric peptidoglycan by PGRP-LE (24, 25). Here, IMD contributes to the delamination of damaged epithelial cells (39), and the expression of immune-regulatory molecules such as the peptidoglycan amidase PGRP-LB (40). Alterations to IMD have been linked to effects on the size and composition of the gut microbiome (16–20), and the lifespan of the fly (41–44). In the adult, IMD also has complex roles in responses to enteric infections. For example, IMD is necessary to survive infections with pathogenic *Serratia marcescens* (45), while IMD accelerates fly demise after infection with *Vibrio cholerae* (31, 32).

Despite our progress in characterizing intestinal IMD, we know comparatively little about cell-specific aspects of IMD activity. For example, several lines of experimental evidence implicate IMD in metabolic homeostasis (17, 46–48), and alterations to lipid metabolism are hallmarks of the generation of anti-bacterial ROS in the intestine (49, 50). However, we don't know if these activities are cell-intrinsic, or if they are secondary to IMD-mediated changes to the gut microbiota. Our results show that inactivation of IMD in distinct cell types has distinct effects on host metabolism. For example, inhibition of IMD in progenitors increases the expression of genes involved in lipid metabolism, and attenuates the expression of genes involved xenobiotic metabolism via glutathione or cytochrome p450. In contrast, inhibition of IMD in enterocytes increases expression of genes required for the transport of amino acids or carboxylic acid, and diminishes the expression of genes required for glycolysis or the metabolism of amino acids. Importantly, the effects of enterocyte IMD on metabolism appear to be independent of the microbiome, as inhibition of enterocyte IMD does not influence bacterial numbers, or microbiome composition. These data suggest that enterocyte IMD has cell-autonomous effects on metabolism. Modification of metabolism by enterocyte IMD has effects on distal sites, as inhibition of enterocyte IMD causes weight gain and hypolipidemia in the adult. Mutations in several IMD pathway genes are also linked to accelerated lipolysis in adult flies (51), further implicating the IMD pathway in the control and use of lipid stores.

The apparent absence of shifts in the microbiome after inhibition of enterocyte IMD was unexpected given the established effects of IMD pathway mutations on the microbiota (16–20). It is possible that these differences reflect a requirement for IMD to act in multiple intestinal cells to modify the gut microbiome. Alternatively, IMD activity in intestinal regions not examined in this study such as the acidic copper cells of the middle midgut may have more pronounced impacts on the microbiome. However, we note that a recent study reported similarities between the microbiome of conventionally reared flies, and immune-deficient *dif* ; *key* mutants (52). Furthermore, immune defects have minimal impacts on the gut microbiome of fish or mice (53, 54). In these models, familial transmission appear to be a major determinant of microbiome composition. As bacteria circulate from the food to the intestine of *Drosophila* (55), we consider it possible that mutations in IMD influence the recycling of symbiotic bacteria, with downstream consequences for the gut microbiome. For example, mutations

in the IMD-responsive NF-kB ortholog, *rel*, affect feeding rates in flies (51), possibly influencing the rate and extent of intestinal colonization by food-resident bacteria.

In contrast to enterocytes, inhibition of IMD in progenitors had detectable effects on intestinal levels of common fly symbitoic *Lactobacillus* species, and no apparent effects on *Acetobacter pasteurianus*. These observations are in keeping with a recent characterization of flies with mutations in *PGRP-SD*, an IMD pathway modifier that is expressed in posterior midgut progenitor cells (27). Loss of PGRP-SD specifically affected intestinal levels of *Lactobacillus plantarum*, but did not affect *Acetobacter pomorum* levels. Thus, it appears that IMD acts in progenitor cells of the midgut to modify host association with *Lactobacillus* symbionts. It will be interesting to see if the effects of IMD on intestinal *Lactobacillus* species are due to alterations in immune tolerance of *Lactobacillus* species, changes in the availability of metabolic intermediates required for bacterial growth, or a combination of those factors.

Mutational inactivation of IMD inhibitors, or chronic activation of IMD results in accelerated growth of the intestinal epithelium (41, 56, 57), although the mechanism remains unclear. Our work establishes IMD as an intrinsic regulator of progenitor growth; inhibition of IMD in the progenitor compartment results in a loss of intestinal progenitors and a decline in epithelial renewal. Recent studies implicate the vertebrate sensor of cytosolic PGN, NOD2, in epithelial regeneration (58, 59), suggesting that immune-regulation of progenitor cell growth may be an evolutionarily conserved event. At present, it is unclear if progenitor cell IMD regulates adult survival by controlling progenitor viability, or proliferation, and future experiments are required to address this question.

Finally, the cell-specific functions of IMD described in this study have consequences for the ability of adult flies to survive infection with the enteric pathogen *Vibrio cholerae*. *imd* mutants survive *V. cholerae* infections longer than wild-type controls (31, 32), indicating a role for IMD in host death. Inhibition of enterocyte IMD recapitulates this phenotype, while inhibition of IMD in progenitors has the opposite effect. These data suggest that enterocyte IMD contributes to *V. cholerae*-dependent killing of the fly, whereas progenitor cell IMD counters the effects of infection. Interestingly, neither phenotype results from changes in bacterial consumption, or the

intestinal load of *V. cholerae*, suggesting that IMD directly affects the ability of flies to tolerate *V. cholerae*. As *V. cholerae* infections are sensitive to metabolite availability (60), and IMD has cell-specific effects on intestinal metabolism, we consider immune-mediated regulation of gut metabolism a candidate mechanism by which IMD influences survival after infection with *V. cholerae*.

In summary, our data suggest that enterocyte IMD influences intestinal, and systemic, metabolism in the fly. Loss of this activity impacts fly weight and lipid levels, and establishes an intestinal environment that favors *V. cholerae* pathogenesis. Progenitor cell IMD activity also affects the expression of metabolic pathway genes, albeit distinct to those controlled by IMD in enterocytes, and establishes an intestinal environment that extends host survival after infection with *V. cholerae*. In the absence of an infectious agent, inhibition of IMD in progenitor cells diminishes the growth and renewal of intestinal progenitors, significantly shortening the lifespan of the fly. Given the evolutionary conservation of immune responses, we believe these data may be of relevance for understanding fundamental principles of immune-regulated intestinal homeostasis.

FIGURE LEGENDS

FIGURE 1. A: qPCR measurement of *dpt* expression in uninfected (mock), or *Ecc15*-infected (*Ecc15*) adult control flies (*R4/+*), or flies that express *imdD30A* in the fat body (*R4/D30A*). Infection experiments were performed with two distinct *imdD30A*-expressing transgenic flies (labeled 1 and 2, respectively). B-C: Survival curves of uninfected (mock), or *V. cholerae*-infected (C6706) adult flies of the indicated genotypes. N=number of flies in each treatment group. Chi-squared and P values are the results of Log-rank tests. D-E: Food consumption rates per adult flies of the indicated genotypes, measured in a CAFÉ assay for the indicated period of days. F-G: CFU/fly of *V. cholerae* in adult flies of the indicated genotypes 24 h after infection with the C6706 strain of *V. cholerae*.

Figure 2. A: Schematic representation of a strategy to generate adult flies with similar populations of symbiotic bacteria. B: Principle component analysis of bacterial OTUs identified in flies of the indicated genotypes and of the indicated ages. C: Faith phylogenetic diversity measurements of bacterial OTUs in flies of the indicated genotypes and ages. Letters above each genotype indicate groups that differ significantly from each other. D: Graphic illustration of replicate quantifications of OTU in flies of the indicated ages and genotypes. E: Heatmap representation of relative bacterial OTU abundance in flies of the indicated ages and genotypes. F: Gneiss analysis was used to identify bacterial balances that differ between treatment groups. G: Bacterial genus abundance in the most significantly distinct bacterial balance.

Figure 3. A-B: Quantification of *Acetobacter pateurianus* (*A.p.*), *Lactobacillus brevis* (*L.b.*), and *Lactobacillus plantarum* (*L.p.*) levels in the intestines of flies of the indicated genotypes raised at 29C for the indicated duration.

Figure 4. A: Schematic representation of an experimental strategy for transcriptomic analysis of dissected midguts from flies with modified IMD pathway activity. B: Principle component analysis of gene expression data for control flies (*Myo1A*^{ts}*/+*), and flies with IMD activity blocked in enterocytes (*Myo1A*^{ts}*/D30A*). C: Volcano plot of genes that

are differentially expressed in *Myo1A*^{ts}/*D30A* midguts relative to *Myo1A*^{ts}/*+* midguts. Each point represents a single gene. Orange indicates genes with a greater than 2 fold-change in gene expression. Green indicates genes with a greater than 2 fold-change in gene expression, and an FDR below 0.01. D: Gene Ontology term analysis of pathways modified by inhibition of IMD in enterocytes. For each pathway, the column indicates the enrichment for the indicated pathway, and the point shows the significance of that enrichment on a negative log scale. E-J: Quantification of glucose (E-F), trehalose (G), triglyceride (H, I), and weight (J) of whole flies, or dissected midguts from flies of the indicated genotypes. All P values indicate results of significance tests performed with Student's t-tests for each measurement. K: Quantification of phospho-histone H3-positive mitotic cells in the posterior midguts of flies of the indicated genotypes raised at 29°C for 28 days. L: Survival curves of control flies (-), or flies with IMD activity blocked in enterocytes (+). N=number of flies tested for each genotype. Chi-squared and P values are the results of Log-rank tests.

Figure 5. A: Principle component analysis of gene expression data for control flies (*esg*^{ts}/*+*), and flies with IMD activity blocked in progenitor cells (*esg*^{ts}/*D30A*). B: Volcano plot of genes that are differentially expressed in *esg*^{ts}/*D30A* midguts relative to *esg*^{ts}/*+* midguts. Each point represents a single gene. Orange indicates genes with a greater than 2 fold-change in gene expression. Green indicates genes with a greater than 2 fold-change in gene expression, and an FDR below 0.01. C: Gene Ontology term analysis of pathways modified by inhibition of IMD in progenitors. For each pathway, the column indicates the enrichment for the indicated pathway, and the point shows the significance of that enrichment on a negative log scale. D: Venn diagrams showing the extent of overlap between genes that are upregulated, or downregulated, in *esg*^{ts}/*D30A* and *Myo1A*^{ts}/*D30A* as indicated. F: Table showing genes involved in immunity; piRNA biogenesis; cholesterol absorption and signaling; signal transduction; proteostasis; and longevity that are differentially regulated in *esg*^{ts}/*D30A* midguts relative to *esg*^{ts}/*+* midguts. Positive scores indicated genes that are upregulated in *esg*^{ts}/*D30A* midguts and negative scores indicate genes that are downregulated. All numerical values indicate the fold-change on a $\log_2$ scale.

Figure 6. A: Percentage of cells positive for the stem cell marker, Delta in the posterior midgut of flies of the indicated genotypes raised at 29°C for the indicated durations. P value indicate results of a significance test performed with a Student's t-test. B: Quantification of phospho-histone H3-positive mitotic cells in the posterior midguts of flies of the indicated genotypes raised at 29°C for 28 days. P value indicates results of a significance test performed with a Student's t-test. L: Survival curves of female control flies (-), or flies with IMD activity blocked in the progenitors (+). N=number of flies tested for each genotype. Chi-squared and P values are the results of Log-rank tests. Survival studies were performed with two distinct *imdD30A*-expressing flies (labeled 1 and 2, respectively).

Supplementary Figure 1: Quantification of total feeding bouts (A-B), number of feeding bursts (C-D), and number of sips (E-F) in adult flies of the indicated genotypes. All flies were raised at 29°C for 23 days prior to the assay, and each point represents the results for a single fly. P-values show the results of unpaired Student's t-tests.

Supplementary Figure 2: Quantification of relative changes in immune gene expression for *Myo1A*^{ts}/*D30A* flies relative to *Myo1A*^{ts}/*+* flies. All measurements were taken from RNAseq data shown in Figure 4, and show the average change on a $\log_2$-fold scale for three biological replicates, as well as P-values and FDR for each gene.

Supplementary Figure 3: Quantification of total triglyceride levels, and body weight for flies of the indicated genotype raised on a holidic diet for 20 days. P-values show the results of unpaired Student's t-tests.

ACKNOWLEDGMENTS

Myo1A^{ts} flies and *esg*^{ts} were provided by Dr. Bruce Edgar. R4GAL4 flies were provided by Dr. Savraj Grewal, and Geneswitch lines were provided by Dr. Heinrich Jasper. The C6706 strain of *Vibrio cholerae* was provided by Dr. Stefan Pukatzki, and *Ecc15* was provided by Dr. Nicolas Buchon. This research was funded by a grant from the Canadian Institutes of Health Research to EF (MOP77746). AP was supported by an AIHS Summer Studentship. We acknowledge microscopy support from Dr. Stephen Ogg at the University of Alberta, and bioinformatics support from Meghan Ferguson and David Fast.

MATERIALS AND METHODS

Fly Husbandry

We used *w*^{1118} as a wildtype strain. We backcrossed *UAS-imdD30A* transgenic lines into the *w*^{1118} background for eight generations prior to use, and used standard fly husbandry methods to ensure that our *esg*^{ts} (*esg-GAL4*, *tub-GAL80*^{ts}, *UAS-GFP*) flies had the same first and third chromosomes as our wild-type line. All fly stocks were maintained at either 18˚C or 25˚C on standard corn meal medium (Nutri-Fly Bloomington formulation, https://bdsc.indiana.edu/information/recipes/bloomfood.html; Genesse Scientific) under a 12h:12h light:dark cycle. All experimental flies were adult virgin females. The *esg*^{ts}*-GAL4, Myo1A*^{ts}*-GAL4* (*Myo1A-GAL4* ; *tub-GAL80*^{ts}, *UAS-GFP*), *5966 GS-GAL4* (RU-486-mediated expression of GAL4 in enterocytes), and *5961 GS-GAL4* (RU-486-mediated expression of GAL4 in progenitor cells) flies were described previously (61–63). The pENTR/D-TOPO Imd construct used in this study was described elsewhere (64). We generated ImdD30A in a two-step site-directed mutagenesis PCR reaction using the following primers: imd-forward (CACCATGTCAAAGCTCAGGAACC), imdD30A-reverse (CCACGGGAGCTGCGGCCTTTTCCAGGCGTCCC), imdD30A-forward (GGGACGCCTGGAAAAGGCCGCAGCTCCCGTGG), imd-reverse (GGAGAAGCGCAAGACAAACAGCTAG). We sequenced the resultant clone (TOPO-ImdD30A) to confirm introduction of the point mutation, and recombined TOPO-ImdD30A with pTW (LR recombination; Invitrogen) to generate the *UASImdD30A* expression plasmids. Transgenic lines were generated by Bestgene Inc. (CA, USA). To make axenic flies, we placed approximately 100 flies of the correct genotypes in a breeding cage with apple juice agar plates that contained yeast paste over night. The following morning, we collected eggs from the apple juice agar plates after visual inspection to confirm absence of larvae, and sterilized them by washing in a 10% solution of 7.4% sodium hypochlorite for 2.5min twice, followed by a 1min washed with 70% EtOH, and three washes with autoclaved water. Working in a tissue-culture hood, we transferred axenic eggs to the surface of autoclaved standard fly food, and transferred vials to a decontaminated incubator at 21˚C under a 12h:12h light:dark cycle. To confirm that flies were axenic, we regularly

sampled the food, by resuspending in MRS (Difco *Lactobacilli* MRS Agar, DB, 288210) and plating onto MRS-agar plates that we checked for bacterial growth after 2-3 days at 29°C.

Adult infections

For septic infection experiments, we grew an overnight culture of *Ecc15* in LB, at 29°C, shaking. We pelleted the overnight culture in 1.5ml microfuge tubes and maintained them on ice. Anesthetized female flies were stabbed under the wing with a needle dipped into the bacterial pellet, control flies were stabbed with a needle dipped into LB. Infected flies were transferred to vials containing regular food overnight. Quantitative PCR (qPCR) measurements were performed with TRIZOL-purified RNA from whole flies (10 per replicate), and we used the DD cycle threshold method to calculate relative expression values. Gene expressions were normalized to actin. The following primers were used in this study: diptericin (F: ACCGCAGTACCCACTCAATC, R: ACTTTCCAGCTCGGTTCTGA), and actin (F: TGCCTCATCGCCGACATAA, R: 59-CACGTCACCAGGGCGTAAT).To test fly survival after oral infection with *V. cholerae*, thirty virgin female flies for each genotype were raised on standard food for 7d at 29°C, then infected with *V. cholerae* C6706 as described previously (31). Briefly, *V. cholerae* were spread on lysogeny broth (LB) agar plates and grown overnight at 37°C. The following morning, 30 flies of each genotype were distributed equally among three empty vials and starved for 2h prior to infection. We then suspended the overnight culture of *V. cholerae* in 10ml fresh LB, and diluted to an OD600 of 0.125. We transferred flies into vials that contained a third of a cotton plug soaked with 3ml of the overnight *V. cholerae* culture. Dead flies were counted every 8h without flipping onto fresh food.

Lifespan assay

For all longevity studies, we used the GeneSwitch (GS) gene expression system to inhibit IMD activity in defined cell types. This system has the advantage that control and experimental populations have identical background genotypes. To activate the GS system, we added 100µl of RU486 (Mifepristone, M8046, Sigma) dissolved in 80% EtOH (4mg/ml) to the surface of standard food and dried overnight prior to addition of flies. For control flies, we

added 100μl of 80% EtOH to the surface of standard food and dried overnight prior to addition of flies. For each treatment group, we placed thirty flies into four vials, for a total of 120 flies per group. All flies were maintained at 25˚C under a 12h:12h light:dark cycle throughout the experiment. We transferred flies to fresh food that contained either RU486, or vehicle, every Monday, Wednesday, and Friday, and counted dead flies at those times.

Establishment of poly-associated gnotobiotic adult *Drosophila*

We generated axenic flies as described above and starved the flies for 2h prior to bacterial poly-association. To generate poly-associated gnotobiotic adults, we fed axenic flies a mix of three *Drosophila* symbiotic bacteria strains (*Lactobacillus plantarum*^{KP}, *Lactobacillus brevis*^{EF}, and *Acetobacter pasteurianus*^{AD}) that were isolated from our wild-type laboratory flies and have described previously (31). Liquid cultures of each bacterial strain were prepared to an OD600 of 50 in 5% sucrose in PBS, then mixed at a 1:1:1 ratio. We placed 25 axenic flies per vial, into 5 vials that contained a quarter of an autoclaved cotton plug soaked with 1ml of bacterial mixture. To poly-associate our flies, we fed flies the bacterial mix for 16h at 29°C. We then raised flies at 29°C on autoclaved standard fly food throughout the remainder of the experiment, transferring to fresh, autoclaved food every Monday, Wednesday, and Friday. To determine CFU at the indicated time points, 25 flies were collected from each group and surface sterilized by successive washes in a 10% solution of 7.4% sodium hypochlorite, distilled water, 70% ethanol, and distilled water respectively. The flies were then randomly divided into groups of 5 and mechanically homogenized in 500μl MRS broth. We serially diluted the homogenate in a 96-well plate, and plated 10μl spots on MRS agar to select for *Lactobacillus* species, or GYC agar to select for *Acetobacter pasteurianus*. Colonies were counted after 2 days growth at 29°C. We distinguished *L. plantarum* and *L. brevis* based on colony morphology: *L. plantarum* forms solid white, opaque colonies, while *L. brevis* colonies were large, round, irregular-edged, with an off-white center and translucent edges. To enumerate *V. cholerae* CFU, we used the procedure described above, working with 7d old virgin female adult flies that we infected with *V. cholerae* at 29°C for 24 hours prior to homogenization in LB buffer.

16S deep-sequencing

For 16S deep-sequencing, we raised axenic fly embryos on autoclaved standard corn meal medium at 21°C. Axenic virgin females were selected, and fed an homogenate prepared from wild-type flies. To prepare the homogenate, we homogenized approximately 3000 adult flies in 50ml of 5% sucrose in PBS. We added 3ml of the homogenate to a third of a cotton plug (Fisher Scientific Canada 14127106) at the base of a clean vial. We transferred axenic flies to each vial (25 flies/vial) and fed flies the homogenate for 16h at 29°C. Flies were transferred to fresh, autoclaved food, and kept on autoclaved food for 5 days or 29 days at 29°C, flipping to fresh food weekly. Flies were surface sterilized, then bacterial DNA was extracted using the UltraClean Microbial DNA Isolation Kit (MO BIO Laboratories, Inc. Catalog #: 12224-250). Bacterial 16S DNA was amplified with PFX Taq (Invitrogen) using 16S pan-bacterial DNA primers (Forward: AGAGTTTGATCCTGGCTCAG, Reverse: GGCTACCTTGTTACGACTT), confirmed by electrophoresis, then purified with the QIAquick PCR Purification Kit (QIAGEN). We measured DNA concentration on Qubit 2.0 then used 1ng of DNA to generate a library with the Nextera PCR Master Mix (Illumina). Libraries were cleaned with AMPure™ beads (QIAGEN), then pooled libraries were processed on the Illumina MiSeq platform with the MiSeq Reagent Kit v3 (600-cycle).

Feeding assay

We performed the Capillary Feeder (CAFE) assays as previously described (65). Briefly, we raised virgin females of the appropriate genotypes 29˚C for 7d. We placed ten flies per vial into vials with three capillaries (calibrated Pipets (5ul, VWR, Cat No. 53432-706)) that contained liquid food with 8.1% sucrose (D-sucrose, Fisher BioReagents, BP220-212) and 1.9% yeast extract (BD, 212750). We measured consumption for ten vials for each genotype. At the same time, we maintained a control vial that contained three food-bearing capillaries, but no flies. To quantify food consumption per fly, we calculated (food consumed in vials that contained flies – food consumed in control vial that lacked flies)/number of flies per fly. We measured total consumption every 24h for 3d. For the FlyPad assay, virgin female adults were aged for 23-24 days at 29˚C (25 flies per vial) with weekly renewal of food. Prior to the FlyPad assay, flies were starved on 1% (w/v) agar for 4h at 29˚C. Flies were placed

into arenas (one fly per arena) with 3µl of food containing 8.1% sucrose, 1.9% yeast extract, and 1% agar. Drosophila feeding behavior was monitored for 1 hour on the FlyPad as described previously (66).

Metabolic assay

For metabolic measurements, adult virgin females were raised on standard medium for 10d at 29˚C. We measured the combined weight of five adult flies then mechanically homogenized in TE buffer (10mM Tris, pH 7.4, 1mM EDTA pH 8.0, 0.1% Triton X-100). The homogenates were used for measuring total triglyceride using the Serum TG Determination Kit (TR0100; Sigma) and total glucose by the GAGO Glucose Assay Kit (GAGO20; Sigma) following the manufacturer's instructions. We performed the same assays with 9-10 dissected intestines from adult virgin females. To measure circulating trehalose, 20 adult flies per sample were punctured on the thorax and spun at 9000 rcf for 5min at 4˚C through a filter tube (Zymo Research, C1006-50-F). Hemolymph was mixed in the trehalase buffer (5 mM Tris pH 6.6, 137 mM NaCl, 2.7 mM KCl) at a 1:100 dilution and heated at 70˚C for 5 min. The mixtures divided into two groups, and one was treated with Porcine Kidney Trehalase (T8778-1UN; Sigma), and another group was not. Both groups were incubated at 37˚C for 22h and treated with glucose assay reagent (GAGO20; Sigma) for 30min at 37˚C. To stop the reaction, we added 12N sulfuric acid and measured absorbance at 540nm.

Immunofluorescence

We used previously described immunofluorescence protocols to visualize posterior midguts (56). In brief, we used anti-phospho-histone H3 (PH3) immunofluorescence to quantify mitoses in the midguts, and anti-Delta immunofluorescence to quantify stem cells in the R4/R5 region of the posterior midguts of virgin female flies that we raised at 29˚C for 5d or 30d. The primary antibodies used in this study were as follows: anti-PH3 (1:1000, Millipore (Upstate), 06-570) mouse anti-Delta (1:100; Developmental Studies Hybridoma Bank C594.9B). For DNA staining we used Hoechst 33258 (1:500; Molecular Probes) and the appropriate secondary antibody are goat anti-mouse Alexa Fluor 647 (1:500,Invitrogen) and 568 (1:500, Invitrogen) and goat anti-rabbit Alexa Fluor 488 (1:1000, Invitrogen) and 546 (1:1300, Invitrogen). Guts were mounted on slides in Fluoromount (Sigma-Aldrich F4680), and

the posterior midgut was visualized with a spinning disk confocal microscope (Quorum WaveFX; Quorum Technologies Inc.). Images were collected as z-slices and processed with Fiji software to generate a single z-stacked image.

Bioinformatics

Statistical analyses for metabolic assays, longevity studies, and survival analyses were performed with GraphPad Prism. Survival data and longevity data were analyzed with Log-rank (Mantal-Cox) tests. Feeding assays, CFU, quantification of PH-3 or Delta positive cells, and metabolic assays were analyzed with unpaired Student's t-tests. Survival, and longevity curves were generated by GraphPad Prism and the R programming language was used for the remaining figures. All figures were assembled using Adobe Illustrator. We used QIIME2-2019.1 (67) for all analysis of 16S data, filtering all sequences that were present below a minimum frequency of 200, and using the DADA2 package for sequence quality control. We binned sequences at 99% sequence identity, and used the greengenes database to identify operational taxonomic units. Differential abundance analysis was performed using the gneiss (68) plugin for QIIME2. RNAseq was performed with RNA purified by TRIZOL (ambion, 15596-026) purification from the midguts of adult flies that we raised at 29°C for 10d. Purified RNA was sent on dry ice to Novogene (CA, USA) for library construction and sequencing with Illumina Platform PE150. For RNAseq studies, we obtained approximately 40 million reads per biological replicate. We used FASTQC (http://www.bioinformatics.bbsrc.ac.uk/projects/fastqc, version 0.11.3) to evaluate the quality of raw, paired-end reads, and trimmed adaptors and reads of less than 36 base pairs in length from the raw reads using Trimmomatic version 0.36 (69). We used HISAT2 version 2.1.0 (70) to align reads to the *Drosophila* transcriptome-bdgp6, and converted the resulting BAM files to SAM flies using Samtools version 1.8 (71). We counted converted files using Rsubread version 1.24.2 (72) and loaded them into EdgeR (73). In EdgeR, we filtered genes with counts less than 1 count per million and normalized libraries for size. Normalized libraries were used to call genes that were differentially expressed among treatments. Genes with P-value < 0.01 and FDR < 0.01 were defined as differentially expressed genes. Principle component analysis was performed on normalized libraries using

Factoextra version 1.0.5 https://CRAN.R-project.org/package=factoextra, and Gene Ontology enRIchment anaLysis and visuaLizAtion tool (GORILLA) was used to determine Gene Ontology (GO) term enrichment (74). Specifically, differentially expressed genes were compared in a two-list unraked comparison to all genes output from edgeR as a background set, and redundant GO terms were removed.

Data availability

Gene expression data have been submitted to the NCBI GEO database (GEO: GSE135154).

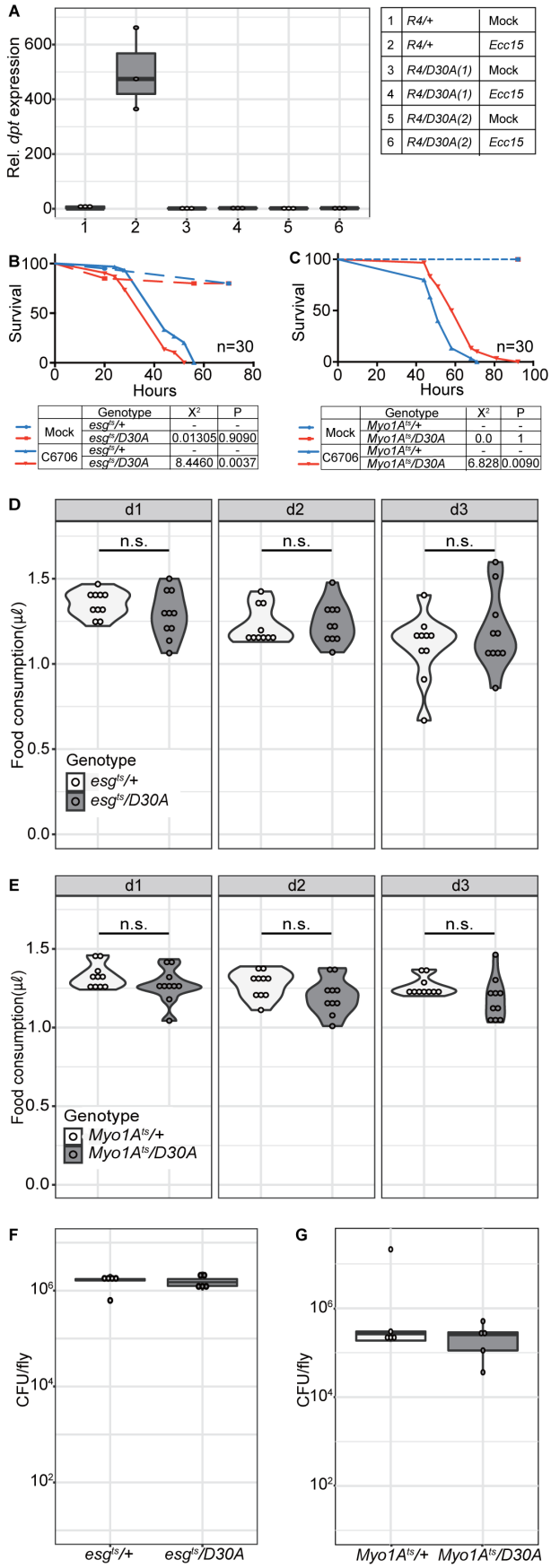
A
Rel. dpt expression
600
400
200
0
1
2
3
4
5
6
1 R4/+ Mock
2 R4/+ Ecc15
3 R4/D30A(1) Mock
4 R4/D30A(1) Ecc15
5 R4/D30A(2) Mock
6 R4/D30A(2) Ecc15
B
Survival
100
50
0
0
20
40
60
80
Hours
n=30
Genotype X² P
Mock esgts/+ - -
esgts/D30A 0.01305 0.9090
C6706 esgts/+ - -
esgts/D30A 8.4460 0.0037
C
Survival
100
50
0
0
20
40
60
80
100
Hours
n=30
Genotype X² P
Mock Myo1Ats/+ - -
Myo1Ats/D30A 0.0 1
C6706 Myo1Ats/+ - -
Myo1Ats/D30A 6.828 0.0090
D
d1
d2
d3
n.s.
n.s.
n.s.
Food consumption(μℓ)
1.5
1.0
0.5
0.0
Genotype
esgts/+
esgts/D30A
E
d1
d2
d3
n.s.
n.s.
n.s.
Food consumption(μℓ)
1.5
1.0
0.5
0.0
Genotype
Myo1Ats/+
Myo1Ats/D30A
F
CFU/fly
10⁶
10⁴
10²
esgts/+
esgts/D30A
G
CFU/fly
10⁶
10⁴
10²
Myo1Ats/+
Myo1Ats/D30A

FIGURE 1

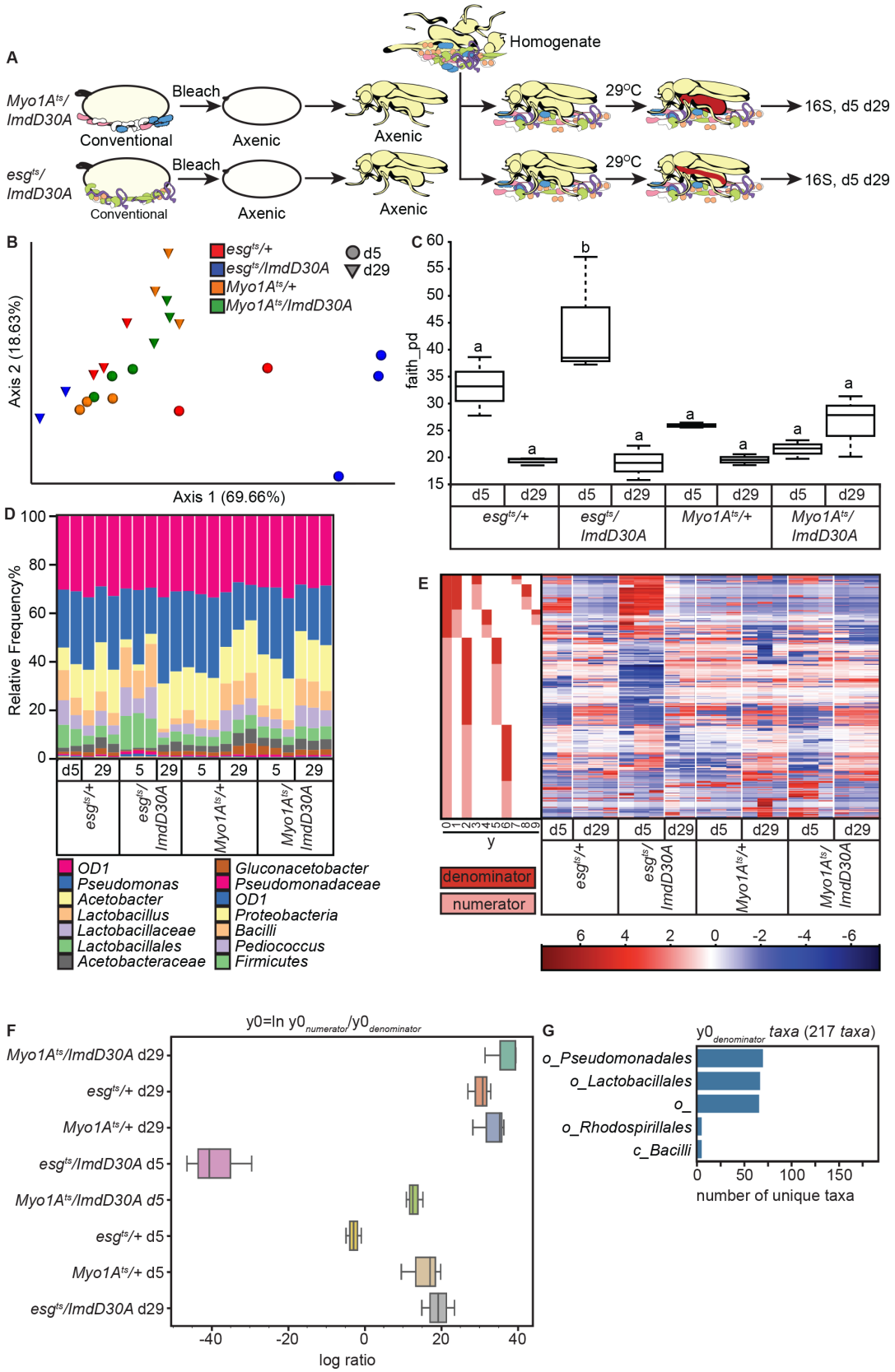
A
Homogenate
Myo1A^ts/ ImdD30A
Bleach
Conventional
Axenic
Axenic
29°C
16S, d5 d29
esg^ts/ ImdD30A
Bleach
Conventional
Axenic
Axenic
29°C
16S, d5 d29
B
esg^ts/+
esg^ts/ImdD30A
Myo1A^ts/+
Myo1A^ts/ImdD30A
d5
d29
Axis 2 (18.63%)
Axis 1 (69.66%)
C
faith_pd
d5
d29
esg^ts/+
esg^ts/ ImdD30A
Myo1A^ts/+
Myo1A^ts/ ImdD30A
D
Relative Frequency%
d5
29
5
esg^ts/+
esg^ts/ ImdD30A
Myo1A^ts/+
Myo1A^ts/ ImdD30A
OD1
Pseudomonas
Acetobacter
Lactobacillus
Lactobacillaceae
Lactobacillales
Acetobacteraceae
Gluconacetobacter
Pseudomonadaceae
OD1
Proteobacteria
Bacilli
Pediococcus
Firmicutes
E
y
denominator
numerator
d5
d29
esg^ts/+
esg^ts/ ImdD30A
Myo1A^ts/+
Myo1A^ts/ ImdD30A
F
y0=ln y0_numerator/y0_denominator
Myo1A^ts/ImdD30A d29
esg^ts/+ d29
Myo1A^ts/+ d29
esg^ts/ImdD30A d5
Myo1A^ts/ImdD30A d5
esg^ts/+ d5
Myo1A^ts/+ d5
esg^ts/ImdD30A d29
log ratio
G
y0_denominator taxa (217 taxa)
o_Pseudomonadales
o_Lactobacillales
o_
o_Rhodospirillales
c_Bacilli
number of unique taxa

FIGURE 2

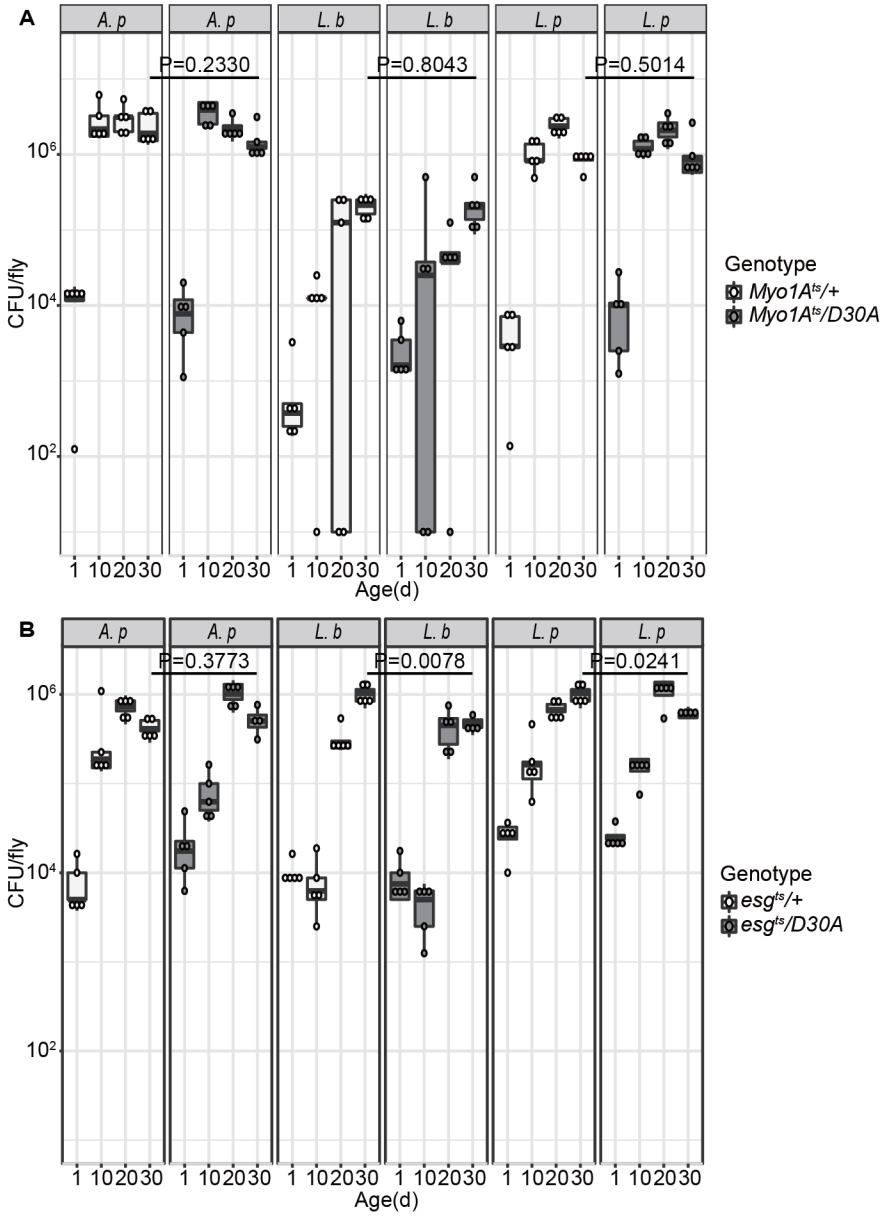
A
A. p
A. p
L. b
L. b
L. p
L. p
P=0.2330
P=0.8043
P=0.5014
CFU/fly
Age(d)
Genotype
Myo1A^ts/+
Myo1A^ts/D30A
B
P=0.3773
P=0.0078
P=0.0241
Genotype
esg^ts/+
esg^ts/D30A

FIGURE 3

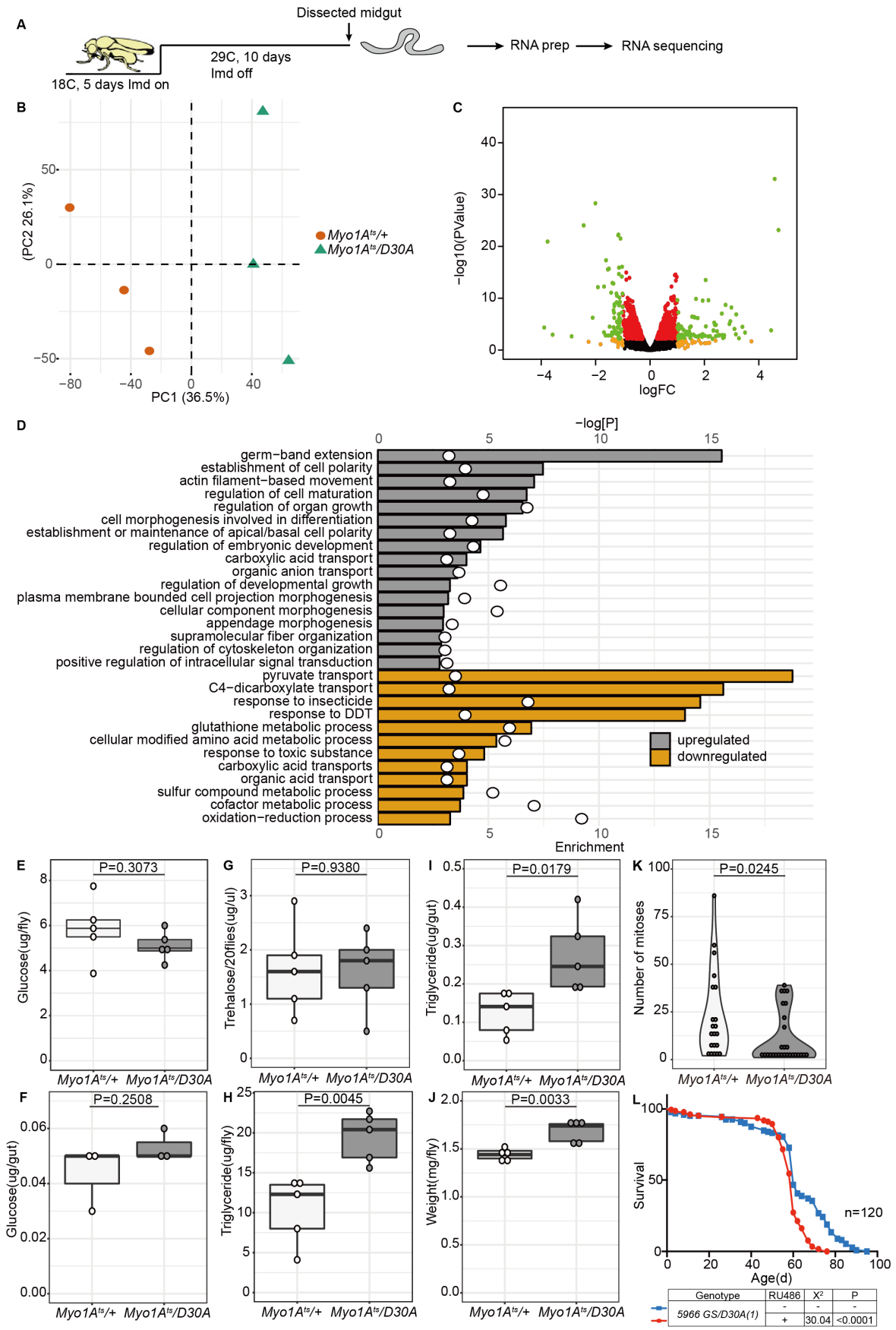
A
Dissected midgut
18C, 5 days Imd on
29C, 10 days
Imd off
RNA prep
RNA sequencing
B
(PC2 26.1%)
PC1 (36.5%)
Myo1A^ts/+
Myo1A^ts/D30A
C
−log10(PValue)
logFC
D
−log[P]
germ−band extension
establishment of cell polarity
actin filament−based movement
regulation of cell maturation
regulation of organ growth
cell morphogenesis involved in differentiation
establishment or maintenance of apical/basal cell polarity
regulation of embryonic development
carboxylic acid transport
organic anion transport
regulation of developmental growth
plasma membrane bounded cell projection morphogenesis
cellular component morphogenesis
appendage morphogenesis
supramolecular fiber organization
regulation of cytoskeleton organization
positive regulation of intracellular signal transduction
pyruvate transport
C4−dicarboxylate transport
response to insecticide
response to DDT
glutathione metabolic process
cellular modified amino acid metabolic process
response to toxic substance
carboxylic acid transports
organic acid transport
sulfur compound metabolic process
cofactor metabolic process
oxidation−reduction process
upregulated
downregulated
Enrichment
E
P=0.3073
Glucose(ug/fly)
G
P=0.9380
Trehalose/20flies(ug/ul)
I
P=0.0179
Triglyceride(ug/gut)
K
P=0.0245
Number of mitoses
F
P=0.2508
Glucose(ug/gut)
H
P=0.0045
Triglyceride(ug/fly)
J
P=0.0033
Weight(mg/fly)
L
Survival
Age(d)
n=120
Genotype | RU486 | X² | P
5966 GS/D30A(1) | - | - | -
+ | 30.04 | <0.0001

FIGURE 4

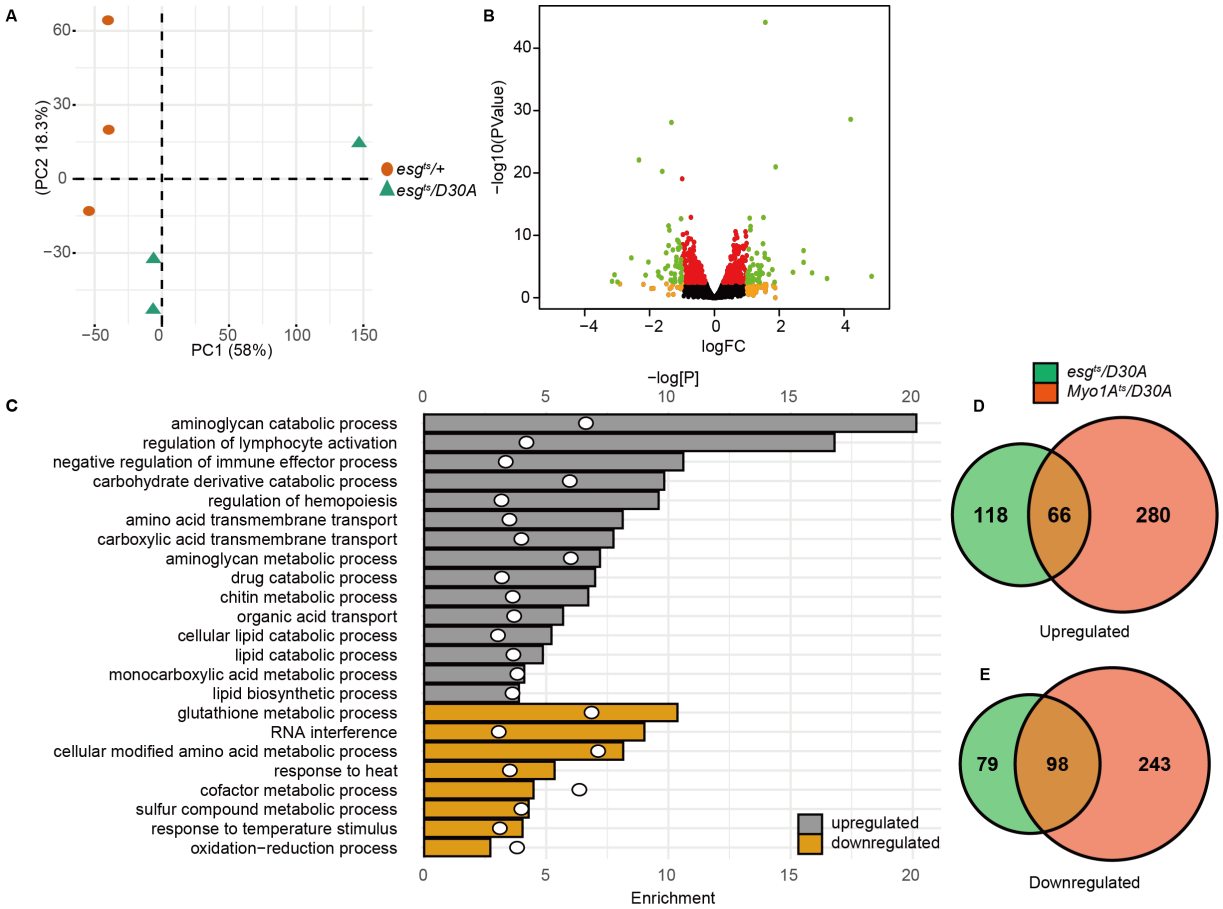

F

Gene	Function	logFC	P-value	Gene	Function	logFC	P-value	Gene	Function	logFC	P-value
IMMUNITY				**METABOLISM**				**PROTEOSTASIS**			
imd	immunity	1.57	7.24E-45	*Hr96*	cholesterol signaling	0.48	8.72E-03	*Ero1L*	protein folding	-0.36	5.00E-03
LysS	immunity	1.18	2.07E-03	*Npc1b*	cholesterol absorption	0.86	4.20E-06	*Ugt*	protein folding	-0.37	1.69E-03
PGRP-SA	immunity	1.09	3.12E-05	*Npc2b*	cholesterol absorption	0.68	2.15E-05	*Der-1*	ERAD pathway	-0.67	1.95E-04
GILT2	immunity	1.03	4.64E-03	*Npc2e*	cholesterol absorption	0.68	2.03E-03	*meigo*	ER stress response	-0.42	2.83E-03
PGRP-SC1a	immunity	1.00	1.82E-07	*Npc1a*	cholesterol absorption	0.41	1.79E-03	*KdelR*	ER stress response	-0.29	6.53E-03
Tep3	immunity	0.88	8.41E-04	**SIGNALING**				*eca*	ER stress response	-0.31	3.27E-03
PGRP-SC1b	immunity	0.84	7.95E-07	*FoxK*	midgut development	-0.30	3.53E-03	*CCT1*	UPR	-0.34	2.28E-03
LysE	immunity	0.80	7.52E-03	*Gp93*	midgut development	-1.01	9.68E-04	*CCT8*	UPR	-0.35	4.77E-04
Rel	immunity	0.61	8.64E-03	*drl*	Wnt	0.41	9.55E-03	*nudC*	UPR	-0.36	5.19E-04
Tehao	immunity	0.57	2.70E-05	*sgg*	Wnt	0.31	2.76E-03	*Herp*	UPR	-0.58	2.63E-04
PGRP-LB	immunity	0.55	1.77E-04	*Cerk*	Wnt	-0.27	4.32E-03	*P58IPK*	UPR	-0.78	2.06E-03
Spn42Dd	immunity	0.55	1.37E-03	*Usp8*	Wnt	-0.32	2.21E-03	*Atg18b*	autophagy	0.75	4.77E-03
Pebp1	immunity	0.41	6.73E-03	*Cdc37*	Wnt	-0.36	5.96E-03	*Atg9*	autophagy	0.29	2.59E-03
Tep4	immunity	0.36	8.82E-04	*boca*	Wnt	-0.40	5.93E-03	*ced-6*	phagocytosis	0.55	8.73E-03
LRR	immunity	0.34	3.40E-03	*p24-1*	Wnt	-0.42	5.81E-03	*drpr*	phagocytosis	0.40	1.72E-03
cactin	immunity	-0.34	1.40E-03	*fz3*	Wnt	-0.46	5.06E-03	**LIFESPAN**			
Sherpa	immunity	-0.56	5.80E-05	*Sec22*	Wnt	-0.53	7.98E-04	*Indy*	metabolism	-0.35	2.44E-03
Vago	immunity	-1.48	6.12E-03	*ebd2*	Wnt	-0.62	2.94E-03	*Coq2*	metabolism	-0.37	5.26E-03
grass	immunity	-1.49	6.47E-08	*Su(var)2-10*	JAK/STAT	-0.32	2.08E-03	*alpha-Est7*	metabolism	-0.40	6.42E-03
Hayan	immunity	-1.63	6.66E-04	*et*	JAK/STAT	-0.72	5.19E-05	*tam*	DNA polymerase	-0.40	3.86E-03
IMPPP	immunity	-2.99	2.98E-03	*Hop*	JAK/STAT	-1.12	1.16E-08	*Cbs*	nitrite reducing	-0.41	4.11E-05
Mekk1	DUOX	0.46	1.54E-05	*kuz*	Notch	0.52	4.51E-03	*Tspo*	mitochondrial	-0.61	8.30E-05
p38c	DUOX	0.41	8.73E-03	*Nedd4*	Notch	0.42	1.59E-05	*Ccs*	SOD activity	-0.70	3.48E-07
PIRNA				*Fkbp14*	Notch	0.31	2.97E-03				
Ars2	piRNA biogenesis	-0.37	1.87E-03	*Nak*	Notch	0.28	6.35E-03				
pasha	piRNA biogenesis	-0.55	1.63E-03	*pzg*	Notch	-0.27	7.02E-03				
armi	piRNA biogenesis	-0.67	1.54E-04	*sno*	Notch	-0.28	6.18E-03				
vret	piRNA biogenesis	-0.79	9.57E-03	*pon*	Notch	-1.00	5.33E-03				

FIGURE 5

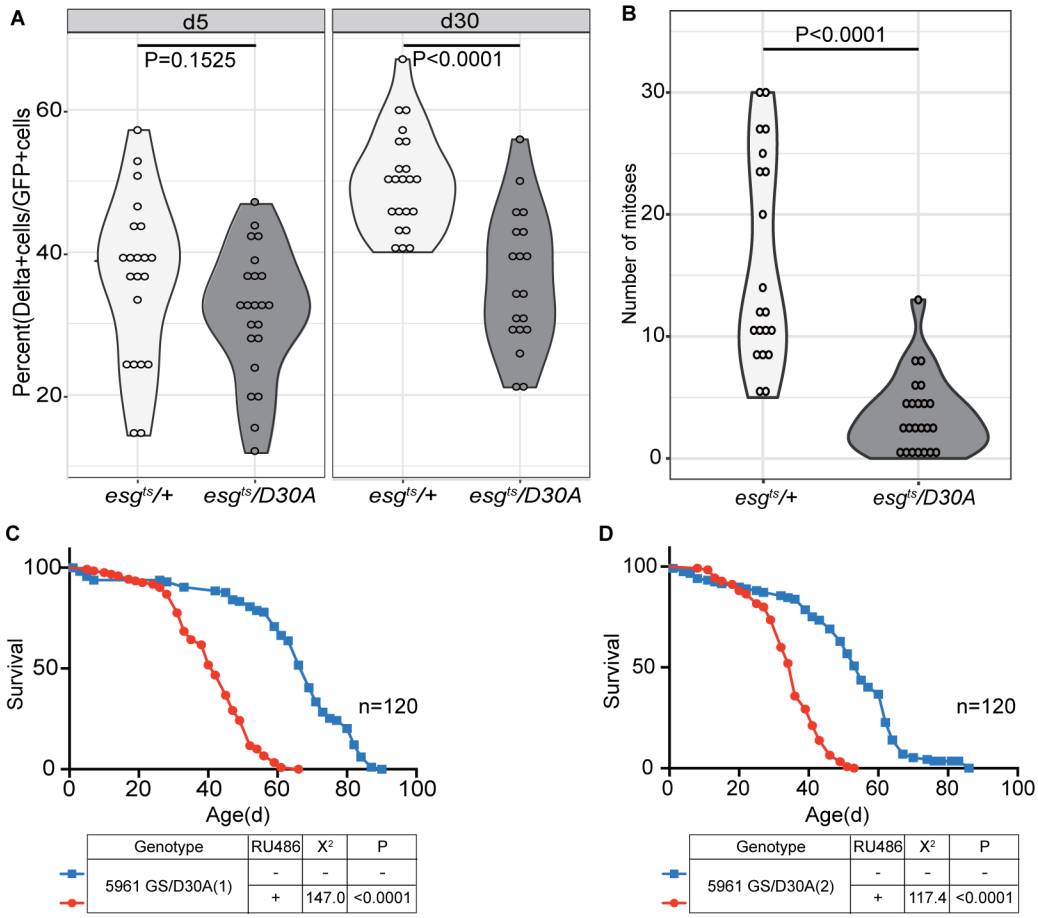
A
d5
d30
P=0.1525
P<0.0001
Percent(Delta+cells/GFP+cells
60
40
20
esg^ts/+
esg^ts/D30A
esg^ts/+
esg^ts/D30A
B
P<0.0001
Number of mitoses
30
20
10
0
esg^ts/+
esg^ts/D30A
C
Survival
100
50
0
n=120
0
20
40
60
80
100
Age(d)
Genotype | RU486 | X² | P
5961 GS/D30A(1) | - | - | -
5961 GS/D30A(1) | + | 147.0 | <0.0001
D
Survival
100
50
0
n=120
0
20
40
60
80
100
Age(d)
Genotype | RU486 | X² | P
5961 GS/D30A(2) | - | - | -
5961 GS/D30A(2) | + | 117.4 | <0.0001

FIGURE 6

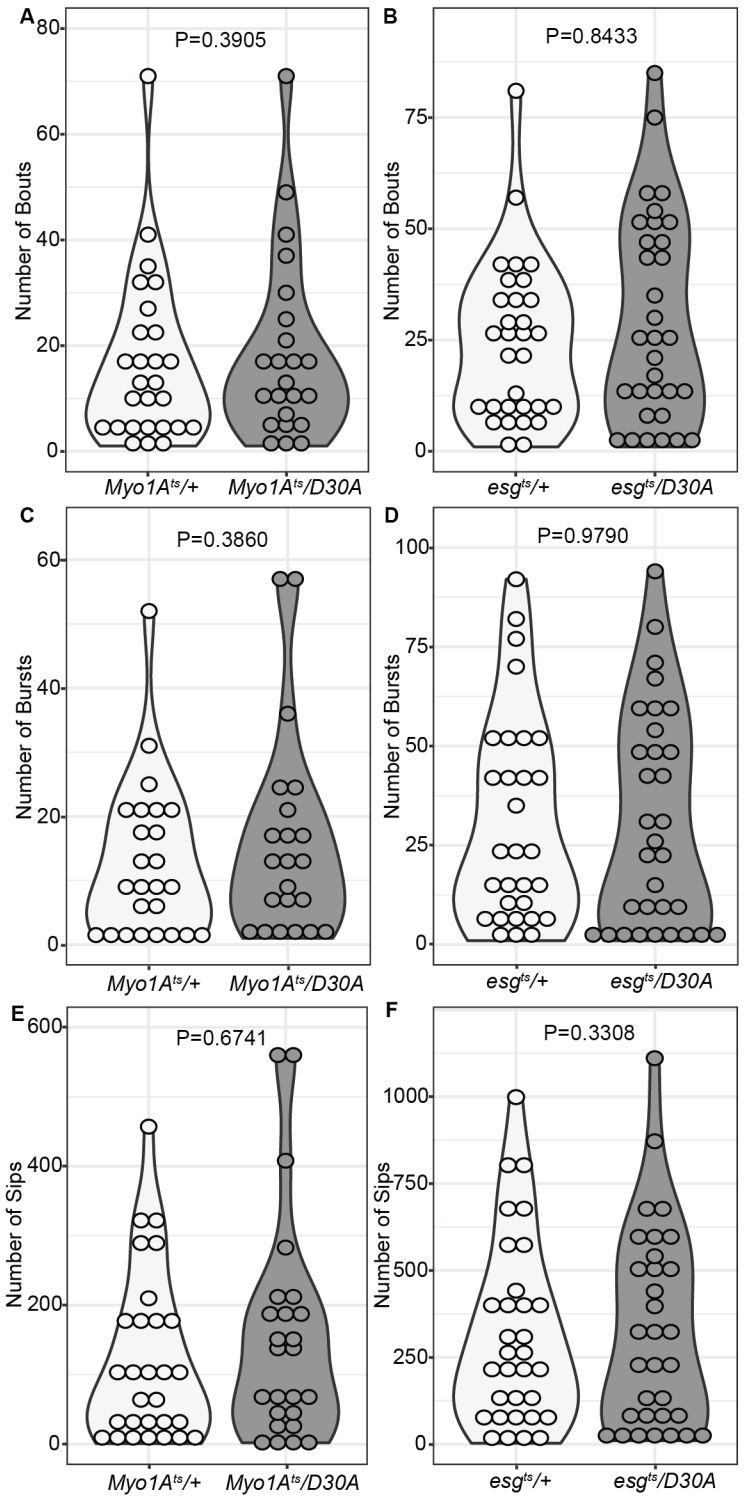

SUPPLEMENTARY FIGURE 1

IMMUNITY			
Gene	logFC	PValue	FDR
AttD	-2.88	2.32E-03	2.32E-02
grass	-1.31	6.30E-07	4.10E-05
Sherpa	-0.51	2.95E-04	5.14E-03
PGRP-LC	-0.36	2.71E-03	2.57E-02
cactin	-0.28	8.87E-03	6.06E-02
GILT1	0.15	3.33E-01	5.81E-01
LRR	0.46	5.49E-05	1.44E-03
PGRP-LB	0.48	1.14E-03	1.39E-02
Tep4	0.52	1.05E-06	6.30E-05
Mekk1	0.55	1.56E-07	1.26E-05
IMPPP	0.61	5.18E-01	7.35E-01
p38c	0.64	4.82E-05	1.30E-03
PGRP-SC1b	0.67	8.00E-05	1.95E-03
Tehao	0.73	5.50E-08	5.08E-06
Rel	0.73	1.66E-03	1.82E-02
LysE	0.81	6.80E-03	4.96E-02
PGRP-SA	0.82	8.94E-04	1.16E-02
Vago	0.83	8.74E-02	2.67E-01
PGRP-SC1a	0.84	1.13E-05	4.36E-04
GILT2	0.94	7.09E-03	5.12E-02
LysS	4.72	6.98E-24	9.48E-21

SUPPLEMENTARY FIGURE 2

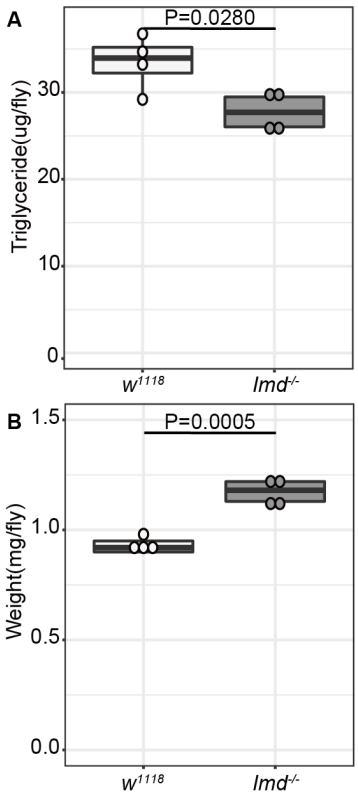

SUPPLEMENTARY FIGURE 3

CITATIONS

1. Hooper L V. (2015) Epithelial Cell Contributions to Intestinal Immunity. *Advances in Immunology* doi:10.1016/bs.ai.2014.11.003.
2. Allaire JM, et al. (2018) The Intestinal Epithelium: Central Coordinator of Mucosal Immunity. *Trends Immunol*. doi:10.1016/j.it.2018.04.002.
3. Miguel-Aliaga I, Jasper H, Lemaitre B (2018) Anatomy and physiology of the digestive tract of drosophila melanogaster. *Genetics*. doi:10.1534/genetics.118.300224.
4. Ohlstein B, Spradling A (2006) The adult Drosophila posterior midgut is maintained by pluripotent stem cells. *Nature* 439(7075):470–474.
5. Micchelli CA, Perrimon N (2006) Evidence that stem cells reside in the adult Drosophila midgut epithelium. *Nature*. doi:10.1038/nature04371.
6. Perdigoto CN, Schweisguth F, Bardin AJ (2011) Distinct levels of Notch activity for commitment and terminal differentiation of stem cells in the adult fly intestine. *Development*. doi:10.1242/dev.065292.
7. Ohlstein B, Spradling A (2007) Multipotent Drosophila intestinal stem cells specify daughter cell fates by differential notch signaling. *Science (80-)*. doi:10.1126/science.1136606.
8. Biteau B, Jasper H (2014) Slit/Robo Signaling Regulates Cell Fate Decisions in the Intestinal Stem Cell Lineage of Drosophila. *Cell Rep*. doi:10.1016/j.celrep.2014.05.024.
9. Zeng X, Hou SX (2015) Enteroendocrine cells are generated from stem cells through a distinct progenitor in the adult Drosophila posterior midgut. *Development*. doi:10.1242/dev.113357.
10. Guo Z, Ohlstein B (2015) Bidirectional Notch signaling regulates Drosophila intestinal stem cell multipotency. *Science (80-)*. doi:10.1126/science.aab0988.
11. Liu X, Hodgson JJ, Buchon N (2017) Drosophila as a model for homeostatic, antibacterial, and antiviral mechanisms in the gut. *PLoS Pathog*. doi:10.1371/journal.ppat.1006277.
12. Jiang H, Edgar BA (2012) Intestinal stem cell function in Drosophila and mice. *Curr Opin Genet Dev*. doi:10.1016/j.gde.2012.04.002.

13. Jiang H, et al. (2009) Cytokine/Jak/Stat Signaling Mediates Regeneration and Homeostasis in the Drosophila Midgut. *Cell*. doi:10.1016/j.cell.2009.05.014.

14. Myllymäki H, Valanne S, Rämet M (2014) The Drosophila Imd Signaling Pathway . *J Immunol*. doi:10.4049/jimmunol.1303309.

15. N. L, et al. (2008) PIMS Modulates Immune Tolerance by Negatively Regulating Drosophila Innate Immune Signaling. *Cell Host Microbe*. doi:10.1016/j.chom.2008.07.004.

16. Buchon N, Broderick NA, Chakrabarti S, Lemaitre B (2009) Invasive and indigenous microbiota impact intestinal stem cell activity through multiple pathways in Drosophila. *Genes Dev*. doi:10.1101/gad.1827009.

17. Broderick NA, Buchon N, Lemaitre B (2014) Microbiota-induced changes in Drosophila melanogaster host gene expression and gut morphology. *MBio*. doi:10.1128/mBio.01117-14.

18. Broderick NA, Lemaitre B (2012) Gut-associated microbes of Drosophila melanogaster. *Gut Microbes*. doi:10.4161/gmic.19896.

19. Ryu JH, et al. (2008) Innate immune homeostasis by the homeobox gene Caudal and commensal-gut mutualism in Drosophila. *Science (80-)*. doi:10.1126/science.1149357.

20. Clark RI, et al. (2015) Distinct Shifts in Microbiota Composition during Drosophila Aging Impair Intestinal Function and Drive Mortality. *Cell Rep*. doi:10.1016/j.celrep.2015.08.004.

21. Buchon N, Broderick NA, Poidevin M, Pradervand S, Lemaitre B (2009) Drosophila Intestinal Response to Bacterial Infection: Activation of Host Defense and Stem Cell Proliferation. *Cell Host Microbe*. doi:10.1016/j.chom.2009.01.003.

22. Ryu J-H, et al. (2004) The Homeobox Gene Caudal Regulates Constitutive Local Expression of Antimicrobial Peptide Genes in Drosophila Epithelia. *Mol Cell Biol*. doi:10.1128/mcb.24.1.172-185.2004.

23. Capo F, Charroux B, Royet J (2016) Bacteria sensing mechanisms in Drosophila gut: Local and systemic consequences. *Dev Comp Immunol*. doi:10.1016/j.dci.2016.01.001.

24. Bosco-Drayon V, et al. (2012) Peptidoglycan sensing by the receptor PGRP-LE in the Drosophila gut

induces immune responses to infectious bacteria and tolerance to microbiota. *Cell Host Microbe*. doi:10.1016/j.chom.2012.06.002.

25. Neyen C, Poidevin M, Roussel A, Lemaitre B (2012) Tissue- and Ligand-Specific Sensing of Gram-Negative Infection in Drosophila by PGRP-LC Isoforms and PGRP-LE . *J Immunol*. doi:10.4049/jimmunol.1201022.

26. Kaneko T, et al. (2006) PGRP-LC and PGRP-LE have essential yet distinct functions in the drosophila immune response to monomeric DAP-type peptidoglycan. *Nat Immunol*. doi:10.1038/ni1356.

27. Iatsenko I, Boquete JP, Lemaitre B (2018) Microbiota-Derived Lactate Activates Production of Reactive Oxygen Species by the Intestinal NADPH Oxidase Nox and Shortens Drosophila Lifespan. *Immunity*. doi:10.1016/j.immuni.2018.09.017.

28. Fink C, et al. (2016) Intestinal FoxO signaling is required to survive oral infection in Drosophila. *Mucosal Immunol*. doi:10.1038/mi.2015.112.

29. Dutta D, et al. (2015) Regional Cell-Specific Transcriptome Mapping Reveals Regulatory Complexity in the Adult Drosophila Midgut. *Cell Rep*. doi:10.1016/j.celrep.2015.06.009.

30. Paquette N, et al. (2010) Caspase-Mediated Cleavage, IAP Binding, and Ubiquitination: Linking Three Mechanisms Crucial for Drosophila NF-κB Signaling. *Mol Cell*. doi:10.1016/j.molcel.2009.12.036.

31. Fast D, Kostiuk B, Foley E, Pukatzki S (2018) Commensal pathogen competition impacts host viability. *Proc Natl Acad Sci*. doi:10.1073/pnas.1802165115.

32. Wang Z, Hang S, Purdy AE, Watnick PI (2013) Mutations in the IMD pathway and mustard counter Vibrio cholerae suppression of intestinal stem cell division in Drosophila. *MBio*. doi:10.1128/mBio.00337-13.

33. McGuire SE, Mao Z, Davis RL (2004) Spatiotemporal Gene Expression Targeting with the TARGET and Gene-Switch Systems in Drosophila. *Sci Signal*. doi:10.1126/stke.2202004pl6.

34. Rodriguez-Fernandez IA, Qi Y, Jasper H (2019) Loss of a proteostatic checkpoint in intestinal stem cells contributes to age-related epithelial dysfunction. *Nat Commun*. doi:10.1038/s41467-019-08982-9.

35. Obniski R, Sieber M, Spradling AC (2018) Dietary Lipids Modulate Notch Signaling and Influence Adult Intestinal Development and Metabolism in Drosophila. *Dev Cell*. doi:10.1016/j.devcel.2018.08.013.

36. Sousa-Victor P, et al. (2017) Piwi Is Required to Limit Exhaustion of Aging Somatic Stem Cells. *Cell Rep*. doi:10.1016/j.celrep.2017.08.059.

37. Ribet D, Cossart P (2015) How bacterial pathogens colonize their hosts and invade deeper tissues. *Microbes Infect*. doi:10.1016/j.micinf.2015.01.004.

38. Zhai Z, Huang X, Yin Y (2018) Beyond immunity: The Imd pathway as a coordinator of host defense, organismal physiology and behavior. *Dev Comp Immunol*. doi:10.1016/j.dci.2017.11.008.

39. Zhai Z, Boquete JP, Lemaitre B (2018) Cell-Specific Imd-NF-κB Responses Enable Simultaneous Antibacterial Immunity and Intestinal Epithelial Cell Shedding upon Bacterial Infection. *Immunity*. doi:10.1016/j.immuni.2018.04.010.

40. Zaidman-Rémy A, et al. (2006) The Drosophila Amidase PGRP-LB Modulates the Immune Response to Bacterial Infection. *Immunity*. doi:10.1016/j.immuni.2006.02.012.

41. Paredes JC, Welchman DP, Poidevin M, Lemaitre B (2011) Negative regulation by Amidase PGRPs shapes the drosophila antibacterial response and protects the Fly from innocuous infection. *Immunity*. doi:10.1016/j.immuni.2011.09.018.

42. Fernando MDA, Kounatidis I, Ligoxygakis P (2014) Loss of Trabid, a New Negative Regulator of the Drosophila Immune-Deficiency Pathway at the Level of TAK1, Reduces Life Span. *PLoS Genet*. doi:10.1371/journal.pgen.1004117.

43. Libert S, Chao Y, Chu X, Pletcher SD (2006) Trade-offs between longevity and pathogen resistance in Drosophila melanogaster are mediated by NFκB signaling. *Aging Cell*. doi:10.1111/j.1474-9726.2006.00251.x.

44. Morris O, et al. (2016) Signal Integration by the IκB Protein Pickle Shapes Drosophila Innate Host Defense. *Cell Host Microbe*. doi:10.1016/j.chom.2016.08.003.

45. Nehme NT, et al. (2007) A model of bacterial intestinal infections in Drosophila melanogaster. *PLoS Pathog*. doi:10.1371/journal.ppat.0030173.

46. Davoodi S, et al. (2019) The Immune Deficiency Pathway Regulates Metabolic Homeostasis in Drosophila

. *J Immunol*. doi:10.4049/jimmunol.1801632.

47. Combe BE, et al. (2014) Drosophila microbiota modulates host metabolic gene expression via IMD/NF-κB signaling. *PLoS One*. doi:10.1371/journal.pone.0094729.

48. Musselman LP, et al. (2017) A Complex Relationship between Immunity and Metabolism in Drosophila Diet-Induced Insulin Resistance . *Mol Cell Biol*. doi:10.1128/mcb.00259-17.

49. Chakrabarti S, Poidevin M, Lemaitre B (2014) The Drosophila MAPK p38c Regulates Oxidative Stress and Lipid Homeostasis in the Intestine. *PLoS Genet*. doi:10.1371/journal.pgen.1004659.

50. Lee KA, et al. (2018) Inflammation-Modulated Metabolic Reprogramming Is Required for DUOX-Dependent Gut Immunity in Drosophila. *Cell Host Microbe*. doi:10.1016/j.chom.2018.01.011.

51. Molaei M, Vandehoef C, Karpac J (2019) NF-κB Shapes Metabolic Adaptation by Attenuating Foxo-Mediated Lipolysis in Drosophila. *Dev Cell*. doi:10.1016/j.devcel.2019.04.009.

52. Mistry R, Kounatidis I, Ligoxygakis P (2017) Interaction between familial transmission and a constitutively active immune system shapes gut microbiota in Drosophila melanogaster. *Genetics*. doi:10.1534/genetics.116.190215.

53. Ubeda C, et al. (2012) Familial transmission rather than defective innate immunity shapes the distinct intestinal microbiota of TLR-deficient mice. *J Exp Med*. doi:10.1084/jem.20120504.

54. Stagaman K, Burns AR, Guillemin K, Bohannan BJM (2017) The role of adaptive immunity as an ecological filter on the gut microbiota in zebrafish. *ISME J*. doi:10.1038/ismej.2017.28.

55. Blum JE, Fischer CN, Miles J, Handelsman J (2013) Frequent replenishment sustains the beneficial microbiome of Drosophila melanogaster. *MBio*. doi:10.1128/mBio.00860-13.

56. Petkau K, Ferguson M, Guntermann S, Foley E (2017) Constitutive Immune Activity Promotes Tumorigenesis in Drosophila Intestinal Progenitor Cells. *Cell Rep*. doi:10.1016/j.celrep.2017.07.078.

57. Guo L, Karpac J, Tran SL, Jasper H (2014) PGRP-SC2 promotes gut immune homeostasis to limit commensal dysbiosis and extend lifespan. *Cell*. doi:10.1016/j.cell.2013.12.018.

58. Zanello G, et al. (2016) The Cytosolic Microbial Receptor Nod2 Regulates Small Intestinal Crypt Damage

and Epithelial Regeneration following T Cell–Induced Enteropathy. *J Immunol*. doi:10.4049/jimmunol.1600185.

59. Nigro G, Rossi R, Commere PH, Jay P, Sansonetti PJ (2014) The cytosolic bacterial peptidoglycan sensor Nod2 affords stem cell protection and links microbes to gut epithelial regeneration. *Cell Host Microbe*. doi:10.1016/j.chom.2014.05.003.

60. Hang S, et al. (2014) The acetate switch of an intestinal pathogen disrupts host insulin signaling and lipid metabolism. *Cell Host Microbe*. doi:10.1016/j.chom.2014.10.006.

61. Nicholson L, et al. (2008) Spatial and temporal control of gene expression in drosophila using the inducible geneSwitch GAL4 system. I. Screen for larval nervous system drivers. *Genetics*. doi:10.1534/genetics.107.081968.

62. Buchon N, Broderick NA, Kuraishi T, Lemaitre B (2010) Drosophila EGFR pathway coordinates stem cell proliferation and gut remodeling following infection. *BMC Biol*. doi:10.1186/1741-7007-8-152.

63. Ren F, et al. (2010) Hippo signaling regulates Drosophila intestine stem cell proliferation through multiple pathways. *Proc Natl Acad Sci*. doi:10.1073/pnas.1012759107.

64. Guntermann S, Foley E (2011) The protein Dredd is an essential component of the c-Jun N-terminal kinase pathway in the Drosophila immune response. *J Biol Chem*. doi:10.1074/jbc.M111.220285.

65. Diegelmann S, et al. (2017) The CApillary FEeder Assay Measures Food Intake in Drosophila melanogaster. *J Vis Exp*. doi:10.3791/55024.

66. Itskov PM, et al. (2014) Automated monitoring and quantitative analysis of feeding behaviour in Drosophila. *Nat Commun*. doi:10.1038/ncomms5560.

67. Rideout JR, et al. (2018) QIIME 2 : Reproducible , interactive , scalable , and extensible microbiome data science. *PeerJ Prepr*. doi:10.7287/peerj.preprints.27295.

68. Morton JT, et al. (2017) Balance Trees Reveal Microbial Niche Differentiation. *mSystems*. doi:10.1128/msystems.00162-16.

69. Bolger AM, Lohse M, Usadel B (2014) Trimmomatic: A flexible trimmer for Illumina sequence data.

Bioinformatics. doi:10.1093/bioinformatics/btu170.

70. Kim D, Langmead B, Salzberg SL (2015) HISAT: A fast spliced aligner with low memory requirements. *Nat Methods*. doi:10.1038/nmeth.3317.

71. Li H, et al. (2009) The Sequence Alignment/Map format and SAMtools. *Bioinformatics*. doi:10.1093/bioinformatics/btp352.

72. Liao Y, Smyth GK, Shi W (2013) The Subread aligner: Fast, accurate and scalable read mapping by seed-and-vote. *Nucleic Acids Res*. doi:10.1093/nar/gkt214.

73. Robinson MD, McCarthy DJ, Smyth GK (2009) edgeR: A Bioconductor package for differential expression analysis of digital gene expression data. *Bioinformatics*. doi:10.1093/bioinformatics/btp616.

74. Eden E, Navon R, Steinfeld I, Lipson D, Yakhini Z (2009) GOrilla: A tool for discovery and visualization of enriched GO terms in ranked gene lists. *BMC Bioinformatics*. doi:10.1186/1471-2105-10-48.